Geomechanics and Engineering, *Vol. 20, No. 4 (2020) 275-285*
DOI: https://doi.org/10.12989/gae.2020.20.4.275

A displacement controlled method for evaluating ground settlement induced by excavation in clay

Jiangu Qian[1,2], Yuanmeng Tong[1,2], Linlong Mu*[1,2], Qi Lu[3] and Hequan Zhao[4]

[1]Department of Geotechnical Engineering, Tongji University, Shanghai 200092, China
[2]Key Laboratory of Geotechnical and Underground Engineering of Ministy of Education, Tongji University, Shanghai 200092, China
[3]Hangzhou Qianjiang New City Construction Development Co., Ltd., Hangzhou 310000, China
[4]China Railway 14th Bureau Group Shield Engineering Co., Ltd, Nanjing, 210000, China

(Received October 9, 2018, Revised November 23, 2019, Accepted January 28, 2020)

Abstract. Excavation usually induces considerable ground settlement in soft ground, which may result in damage of adjacent buildings. Generally, the settlement is predicted through elastic-plastic finite element method and empirical method with defects. In this paper, an analytical solution for predicting ground settlement induced by excavation is developed based on the definition of three basic modes of wall displacement: T mode, R mode and P model. A separation variable method is employed to solve the problem based on elastic theory. The solution is validated by comparing the results from the analytical method with the results from finite element method(FEM) and existing measured data. Good agreement is obtained. The results show that T mode and R mode will result in a downward-sloping ground settlement profile. The P mode will result in a concave-type ground settlement profile.

Keywords: excavation; ground settlement; retaining wall movement; analytical solution; displacement-controlled method

1. Introduction

With the developments of high-rise buildings, subway rail transits and underground spaces in urban area, the influence of the excavation on the surrounding environment attracts many attentions. The soil movement induced by the excavation usually determines the damage potential of the buildings adjacent to the excavation (Finno and Bryson 2002). Most infrastructures and buildings are supported by shallow foundations. The damage potential of those building induced by excavation can be determined from the corresponding ground surface settlement (Poulos 1997).

Many experiments have been carried out to evaluate the ground surface settlement induced by the excavation, including in-situ tests (Clough and O'Rourke 1990, Hong *et al.* 2015, Kim and Jung 2016, Tan *et al.* 2017, He *et al.* 2018), laboratory model tests (Seok *et al.* 2001, Lam 2010) and centrifuge tests (Nomoto *et al.* 1999, Wang *et al.* 2012a). Two typical ground settlement types are found based on those test data: spandrel type and concave type (Hsien and Ou 1998, Ou *et al.* 1993). It is now commonly recognized that the problem can be assumed as plan strain problem when evaluating the maximum deformation induced by the excavation (Finno and Harahap 1991, Wang *et al.* 2012b). Plenty of empirical methods have been proposed based on those experimental data to predict the ground settlement induced by the excavation (Roboski and Finno 2006, Kung *et al.* 2007, Wang *et al.* 2009, Ou and Hsieh 2011, Golpasand *et al.* 2016). In those empirical methods, the ground settlements are generally calculated from the deflections of the retaining wall. Unfortunately, empirical methods are data based. Their applicability is regionally restricted. Besides, numerical methods, such as FEM, are widely used as well (Hashash and Whittle 1996, Arai *et al.* 2008, Zahmatkesh and Choobbasti 2015, Chen *et al.* 2018). FEM has advantages in simulating complex boundary conditions and capturing the deformation both in small and large range(Mu and Huang 2016). While, the quality of FEM highly depends on the soil model and the input parameters(Mu *et al.* 2015). Moreover, the requirements of a high quality FEM analysis are usually too high for engineers. An analytical method may explain the mechanism clearly and make the prediction easier. It is widely proved that elastic theory could significantly simplify foundation problems and give solutions that reasonably meet the engineer requirements, especially for displacement boundary problems(Poulos and Davis 1974). For example, settlement of foundation induced by surface loadings and ground surface(Sheehan *et al.* 2010) induced by tunnelling(Loganathan and Poulos 1998). However, no existing analytical method for predicting the ground settlement induced by excavations has been found due to the complex of the excavation according to the author's knowledge.

Many efforts have been made to estimate the maximum deflection of the retaining wall of the excavation(Wang *et al.* 2012a, Liu *et al.* 2015). They are approved to be usable to predict the maximum deflection of the retaining wall induced by the excavation. The aim of this paper is to

*Corresponding author, Associate Professor
E-mail: mulinlong@tongji.edu.cn

ISSN: 2005-307X (Print), 2092-6219 (Online)

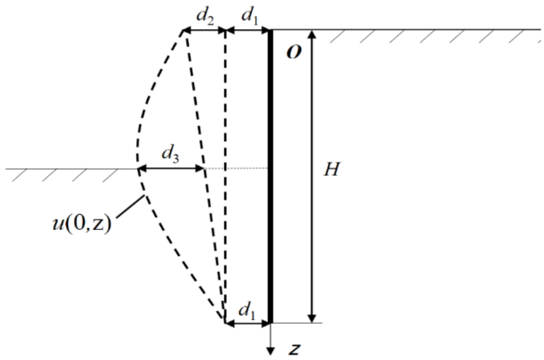

Fig. 1 Schematic of the surface subsidence caused by an excavation

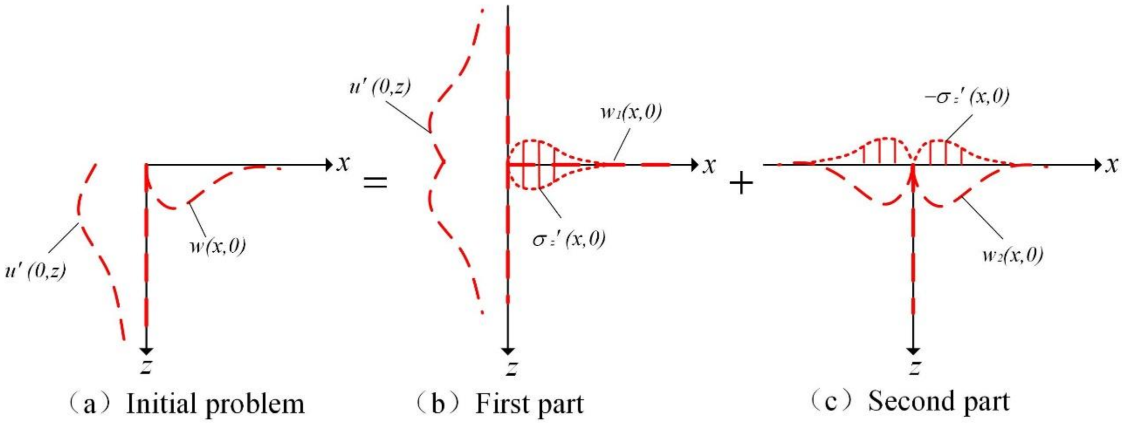

Fig. 2 Mirror symmetry principle for solving excavation-induced ground movement

calculate the ground surface settlement induced by the excavation based on the deflection of the retaining wall obtained by the existing method through a displacement-controlled method(DCM). In this paper, three boundary conditions of excavation are defined by analyzing the boundary conditions of the excavation firstly according to the existing researches. The settlement of the ground is solved by elastic theory coupled with mirror symmetry principle based on three boundary conditions defined herein.

2. General theory

In order to get the maximum deformation induced by the excavation, the problem is assumed as a plane strain problem. As shown in Fig.1, the horizontal displacement of the retaining wall consists of three parts:(1) translation;(2) rotation around the wall toe; (3) parabola deformation. In Fig. 1, H is the wall depth, $u(0,z)$ is the horizontal deformation of the retaining wall, d_1, d_2 and d_3 are the maximum horizontal deformation of the retaining wall under translation, rotation and parabola deformation respectively. Three assumptions are made:(1)Soil movement behind the retaining wall is caused by the horizontal deformation of the retaining wall which can be obtained from existing methods (Mu and Huang 2016). The horizontal deformation of the retaining wall is assumed to be the boundary condition of the problem when solving the problem using DCM. The vertical movement of the soil caused by the frictional stress between the wall and the soil is neglected. Thus, the frictional stress between the wall and the soil is neglected. (2)The soil is homogenous and linear elasticity. Although many researches shows plastic behavior of the soil should be considered to calculate the soil movement induced by the excavation accurately, Kyrou (1980) showed that the error caused by using the elastic model for soil is engineering acceptable when evaluating the influence of excavations on adjacent pipeline. Unlike the force control method(FCM) which relies on soil constitutive model significantly, Cheng *et al.* (2007) showed that DCM can calculate the deformation induced by tunnel excavation by using a simple soil constitutive model. Many researches(Loganathan and Poulos 1998, Mu *et al.* 2012) also shows that deformation caused by excavation problems can be correctly calculated by DCM even when the initial stress is not considered in the problem. Thus, we employ elastic theory to significantly simplify the problem to make it applicable to engineers; however it will lead to engineering acceptable error. (3) The ground deformation below the retaining wall is negligible.

A mirror symmetry principle is employed in this analysis as schematically shown in Fig. 2. The ground settlement behind the retaining wall could be calculated by two steps. First step: calculate the free field movement of soil caused by the horizontal deflection of the retaining wall as shown in Fig.2(b). At this step, the vertical displacement on the ground surface is 0. It indicates that the ground surface can be assumed to be the symmetrical plane of the problem shown in the first part. Secondly, apply the normal stress σ_x produced by the first step onto the surface inversely by using the retaining wall as the symmetrical plane. Adding the deformation induced by those two parts together, the ground settlement induced by the excavation can be obtained.

In Fig.2, the deformation of the first part could be solved by Lame's equation for a plane strain problem without considering the body force(Pasternak *et al.* 2004). The Lame's equation in x and z directions could be expressed as:

$$\begin{cases}(\lambda+2G)\dfrac{\partial^2 u}{\partial x^2}+G\dfrac{\partial^2 u}{\partial z^2}+(\lambda+G)\dfrac{\partial^2 w}{\partial x\partial z}=0\\(\lambda+2G)\dfrac{\partial^2 w}{\partial z^2}+G\dfrac{\partial^2 w}{\partial x^2}+(\lambda+G)\dfrac{\partial^2 u}{\partial x\partial z}=0\end{cases}\tag{1}$$

where λ and G are the Lame's elastic coefficients, $\lambda=\dfrac{E\upsilon}{(1+\upsilon)(1-2\upsilon)}$ and $G=\dfrac{E}{2(1+\upsilon)}$.

In order to solve Eq. (1), the following transformation is introduced.

$$\begin{cases}\theta=\dfrac{\partial u}{\partial x}+\dfrac{\partial w}{\partial z}\\\omega=\dfrac{1}{2}\left(\dfrac{\partial w}{\partial x}-\dfrac{\partial u}{\partial z}\right)\end{cases}\tag{2}$$

where θ is the volumetric strain, ω is the rigid body rotation angle.

From the Eq. (1) and Eq. (2), the following equations can be obtained.

$$\begin{cases}(\lambda+2G)\dfrac{\partial\theta}{\partial x}-2G\dfrac{\partial\omega}{\partial z}=0\\(\lambda+2G)\dfrac{\partial\theta}{\partial z}+2G\dfrac{\partial\omega}{\partial x}=0\end{cases}\tag{3}$$

Deriving Eq. (3) for x and z separately. Then we can get Eq. (4).

$$\begin{cases}\nabla^2\theta=0\\\nabla^2\omega=0\end{cases}\tag{4}$$

where $\nabla^2=\dfrac{\partial^2}{\partial x^2}+\dfrac{\partial^2}{\partial z^2}$.

Using the separation variable method, the general solution for Eq. (4) can be obtained.

$$\begin{cases}\theta=\dfrac{\partial u}{\partial x}+\dfrac{\partial w}{\partial z}=\displaystyle\int_0^{+\infty}\left[A_1\cos(\alpha z)+A_2\sin(\alpha z)\right]\left(K_1'e^{-\alpha x}+K_2'e^{\alpha x}\right)d\alpha\\\omega=\dfrac{\partial u}{\partial z}-\dfrac{\partial w}{\partial x}=\displaystyle\int_0^{+\infty}\left[B_1\cos(\alpha z)+B_2\sin(\alpha z)\right]\left(K_3'e^{-\alpha x}+K_4'e^{\alpha x}\right)d\alpha\end{cases}\tag{5}$$

According to the boundary condition that θ=0 and ω =0 when x=+∞, we can get $K_2'=K_4'=0$. Set $A_1'=K_1'A_1$, $A_2'=K_1'A_2$, $B_1'=K_3'B_1$, $B_2'=K_3'B_2$.

Then,

$$\begin{cases}\theta=\displaystyle\int_0^{+\infty}\left[A_1'\cos(\alpha z)+A_2'\sin(\alpha z)\right]e^{-\alpha x}d\alpha\\\omega=\displaystyle\int_0^{+\infty}\left[B_1'\cos(\alpha z)+B_2'\sin(\alpha z)\right]e^{-\alpha x}d\alpha\end{cases}\tag{6}$$

Combined Eq. (6), (3) and (4), we can get

$$\begin{cases}\nabla^2 u=\left(-\dfrac{\lambda+2\mu}{2\mu}-1\right)\displaystyle\int_0^{+\infty}\alpha\left[A'_1\cos(\alpha z)+A'_2\sin(\alpha z)\right]e^{-\alpha x}d\alpha=0\\\nabla^2 w=\left(-\dfrac{\lambda+2\mu}{2\mu}-1\right)\displaystyle\int_0^{+\infty}\alpha\left[A'_1\sin(\alpha z)-A'_2\sin(\alpha z)\right]e^{-\alpha x}d\alpha=0\end{cases}\tag{7}$$

The general solution for Eq. (7) can be written as

$$\begin{cases}u=\displaystyle\int_0^{+\infty}\dfrac{1}{\alpha}\left[K_1\cos(\alpha z)+K_2\sin(\alpha z)\right](A+B\alpha x)e^{-\alpha x}d\alpha\\w=\displaystyle\int_0^{+\infty}\dfrac{1}{\alpha}\left[-K_2\cos(\alpha z)+K_1\sin(\alpha z)\right](C+D\alpha x)e^{-\alpha x}d\alpha\end{cases}\tag{8}$$

Substituting Eq. (8) into Eq. (1), we can get

$$\begin{cases}u=\displaystyle\int_0^{+\infty}\dfrac{1}{\alpha}\left[K_1\cos(\alpha z)+K_2\sin(\alpha z)\right](A+B\alpha x)e^{-\alpha x}d\alpha\\w=\displaystyle\int_0^{+\infty}\dfrac{1}{\alpha}\left[-K_2\cos(\alpha z)+K_1\sin(\alpha z)\right](C+D\alpha x)e^{-\alpha x}d\alpha\end{cases}\tag{9}$$

The stress can be expressed as:

$$\begin{cases}\sigma_x=(\lambda+2G)\dfrac{\partial u}{\partial x}+\lambda\dfrac{\partial w}{\partial z}\\\sigma_z=(\lambda+2G)\dfrac{\partial w}{\partial z}+\lambda\dfrac{\partial u}{\partial x}\\\tau_{xz}=G\left(\dfrac{\partial u}{\partial z}+\dfrac{\partial w}{\partial x}\right)\end{cases}\tag{10}$$

Based on the boundary condition, $\tau_{xz|z=0}=0$, we can get that K_2=0. And define K_3=K_1·A. Eq. (9) can be written as following:

$$\begin{cases}u=\displaystyle\int_0^{+\infty}\dfrac{1}{\alpha}\cos\alpha z(K_3+K_1\alpha x)e^{-\alpha x}\mathrm{d}\alpha\\w=\displaystyle\int_0^{+\infty}\dfrac{1}{\alpha}\sin\alpha z(K_3-K_1\dfrac{\lambda+3G}{\lambda+G}+K_1\alpha x)e^{-\alpha x}\mathrm{d}\alpha\end{cases}\tag{11}$$

where K_1 and K_3 are the coefficients depend on the boundary conditions.

And Eq. (10) can be written as:

$$\begin{cases}\sigma_x=2G\displaystyle\int_0^{+\infty}\left[(1-\alpha x)K_1-\dfrac{\lambda}{\lambda+G}K_1-K_3\right]\cos(\alpha z)e^{-\alpha x}d\alpha\\\sigma_z=2G\displaystyle\int_0^{+\infty}\left(-\dfrac{2\lambda+3G}{\lambda+G}K_1+K_1\alpha x+K_3\right)\cos(\alpha z)e^{-\alpha x}d\alpha\\\tau_{xz}=G\displaystyle\int_0^{+\infty}\left[(1-2\alpha x)K_1+\dfrac{\lambda+3G}{\lambda+G}K_1-2K_3\right]\sin(\alpha z)e^{-\alpha x}d\alpha\end{cases}\tag{12}$$

The frictional stress between soil and structure is neglected, $\tau_{xz|x=0}$=0, we can get Eq. (13) from Eq. (12).

$$K_3=\frac{\lambda+2G}{\lambda+G}K_1\tag{13}$$

Substituting Eq.(13) into Eq.(11), we get

$$\begin{cases}u=\displaystyle\int_0^{+\infty}\dfrac{1}{\alpha}\cos(\alpha z)(1+\dfrac{\lambda+G}{\lambda+2G}\alpha x)K_3e^{-\alpha x}\mathrm{d}\alpha\\w=\displaystyle\int_0^{+\infty}\dfrac{1}{\alpha}\sin(\alpha z)(-\dfrac{G}{\lambda+2G}+\dfrac{\lambda+G}{\lambda+2G}\alpha x)K_3e^{-\alpha x}\mathrm{d}\alpha\end{cases}\tag{14}$$

The horizontal displacement of soil at the vertical plan of retaining wall, where x=0, is:

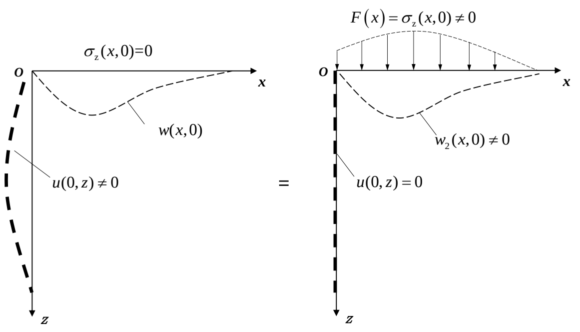

Fig. 3 Actual surface subsidence is equal to the second surface subsidence

$$
\begin{aligned}
u(0,z) &= \int_0^{+\infty} \frac{1}{\alpha}\cos(\alpha z) K_3 \,\mathrm{d}\alpha \\
&= \int_0^{+\infty} \frac{1}{2\alpha}(e^{i\alpha z}+e^{-i\alpha z}) K_3 \,\mathrm{d}\alpha \\
&= \int_{-\infty}^{+\infty} \frac{1}{2\alpha} e^{i\alpha z} K_3 \,\mathrm{d}\alpha
\end{aligned}
\tag{15}
$$

According to *Fourier* cosine integral transformation,

$$u(0,z) = \frac{1}{2\pi}\int_{-\infty}^{+\infty} e^{i\alpha z}\,\mathrm{d}\alpha \tag{16}$$

Comparing Eq. (15) and Eq. (16), it is easy to find:

$$K_3 = \frac{\alpha}{\pi} \tag{17}$$

The vertical displacement at the ground surface in the first part, as shown in Fig. 2(b), is 0, $w_1(x,0)=0$. Therefore, the surface settlement caused by horizontal deformation of the retaining wall, $w(x,0)$, is equal to the settlement of the second part caused by the positive surface stress, $w_2(x,0)$, as shown in Fig. 3. The calculation of $w_2(x,0)$ will be introduced in the following section according to the specific deformation modes of retaining wall.

3. Solutions for specific boundary modes

3.1 Translation mode (T mode)

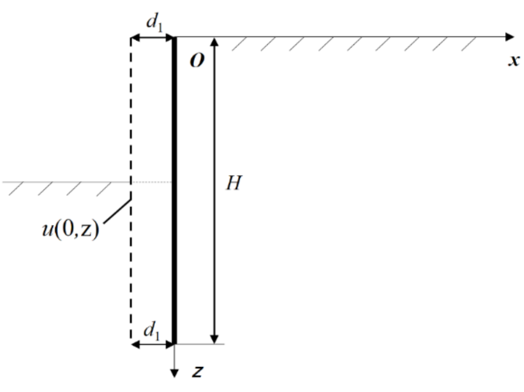

Fig. 4 Boundary condition of T mode

As shown in Fig. 4, the boundary conditions for translation mode is that $u(0,z)=-d_1$ when $0\le z\le H$.

$$u = \int_0^{+\infty} \frac{1}{\alpha} K_3 \cos(\alpha z)\,\mathrm{d}\alpha = -d_1 \tag{18}$$

According to *Fourier* cosine integral transformation, we can get:

$$-d_1 = -\frac{2d_1}{\pi}\int_0^{+\infty} \frac{\sin(H\alpha)}{\alpha}\cos(\alpha z)\,\mathrm{d}\alpha \tag{19}$$

Comparing (18) and (19), it can get:

$$K_3 = -\frac{2d_1}{\pi}\sin(H\alpha) \tag{20}$$

Substituting Eq.(20) into Eq.(14), we get

$$
\begin{cases}
u = -\dfrac{2d_1}{\pi}\displaystyle\int_0^{+\infty}\frac{1}{\alpha}\cos(\alpha z)(1+\frac{\lambda+G}{\lambda+2G})\sin(H\alpha)e^{-\alpha x}\mathrm{d}\alpha \\
w = -\dfrac{2d_1}{\pi}\displaystyle\int_0^{+\infty}\frac{1}{\alpha}\sin(\alpha z)(1+\frac{\lambda+G}{\lambda+2G}\alpha x-\frac{\lambda+3G}{\lambda+2G})\sin(H\alpha)e^{-\alpha x}\mathrm{d}\alpha
\end{cases}
\tag{21}
$$

For the first part, the settlement at the ground surface is 0, $w|_{z=0}=0$.

Substituting Eq. (13) and Eq. (20) into Eq. (12),

$$
\begin{cases}
\sigma_x = \dfrac{d_1}{2\beta\pi}\left\{\dfrac{z+H}{(z+H)^2+x^2}+\dfrac{2(z+H)x^2}{\left[(z+H)^2+x^2\right]^2}\right. \\
\qquad\left.-\dfrac{z-H}{(z-H)^2+x^2}-\dfrac{2(z-H)x^2}{\left[(z-H)^2+x^2\right]^2}\right\} \\
\sigma_z = \dfrac{d_1}{2\beta\pi}\left\{\dfrac{z+H}{(z+H)^2+x^2}-\dfrac{2(z+H)x^2}{\left[(z+H)^2+x^2\right]^2}\right. \\
\qquad\left.-\dfrac{z-H}{(z-H)^2+x^2}+\dfrac{2(z-H)x^2}{\left[(z-H)^2+x^2\right]^2}\right\} \\
\tau_{xz} = \dfrac{d_1}{2\beta\pi}x\left\{\dfrac{x^2-(H-z)^2}{\left[x^2+(H-z)^2\right]^2}-\dfrac{x^2-(H+z)^2}{\left[x^2+(H+z)^2\right]^2}\right\}
\end{cases}
\tag{22}
$$

At the ground surface, z=0,

$$\sigma_{z|z=0} = \frac{d_1H(H^2-x^2)}{\beta\pi(x^2+H^2)^2} \tag{23}$$

where $\beta=\dfrac{1-G^2}{E}$.

Thus, the inverse stress acting on the surface in part 2, as shown in Fig. 3, can be expressed as follows

$$F(x) = -\frac{d_1H(H^2-x^2)}{\beta\pi(x^2+H^2)^2} \tag{24}$$

According to *Boussinesq-Flamant* solution for plane strain problem, the surface settlement caused by a concentrated load P is:

$$w = \frac{2\beta P}{\pi}\ln\frac{s}{\rho} \tag{25}$$

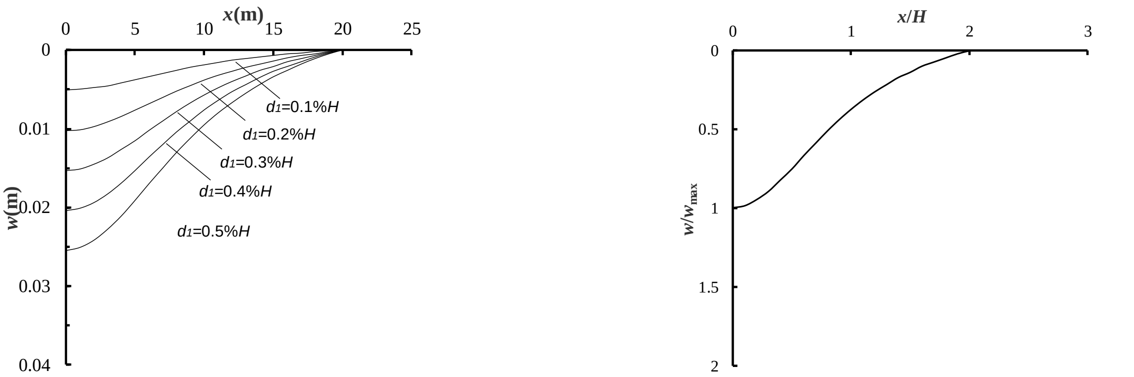

(a) Surface subsidence curves (b) Normalized curve of surface subsidence

Fig. 5 Surface subsidence distribution under translation of retaining wall

where $\rho=|x_c-x|$, $s=|x_c-x_{ref}|$. For a strict elasticity theory, $x_{ref}=\infty$. However, it is well recognized that the ground settlement induced by the excavation usually occurs in a zone, which is about 4 time the excavation depth away from the retaining wall (Kung *et al.* 2007). In soft ground area, the depth of the retaining wall is usually twice the excavation depth. The ground settlement induced by the excavation beyond the influence zone can be neglect. The settlement of the ground surface in the influence zone is focused in practice. In order to focus on the main deformation that has significant effect on engineering, the method is focused to the deformation in the influence zone. Thus, x_{ref} is defined as $2H$ herein.

Substituting Eq. (24) into Eq. (25), the ground surface settlement induced by $F(x)$ is:

$$w(x)=-\frac{2d_1H}{\pi^2}\int_{-\infty}^{+\infty}\frac{x_c^{\ 2}-H^2}{(x_c^{\ 2}+H^2)^2}\ln\left|\frac{x_c-x}{x_c-x_{ref}}\right|\mathrm{d}\,x_c \tag{26}$$

Thus, the ground surface induced by the deformation of the retaining wall is:

$$w(x)=\frac{2d_1H^2}{\pi}\left(\frac{1}{x^2+H^2}-\frac{1}{x_{ref}^{\ 2}+H^2}\right) \tag{27}$$

Defining H=10 m, the ground surface settlements corresponding to d_1 = 0.1%H, 0.2%H, 0.3%H, 0.4%H and 0.5%H are shown in Fig.5(a). And the normalized ground surface settlement are shown in Fig. 5(b). It can be see that the magnitude of the wall deformation does not influence the distribution of the ground surface settlement when the wall deforms according to T mode. The magnitude of the wall deformation only influences the maximum ground surface settlement.

Let the first derivative of $w(x)$ equals 0, the maximum settlement can be obtained by the following equation. Correspondingly, the maximum settlement locates at the location where x=0.

$$w_{\max}=\frac{2d_1H^2}{\pi}\left(\frac{1}{H^2}-\frac{1}{x_{ref}^{\ 2}+H^2}\right) \tag{28}$$

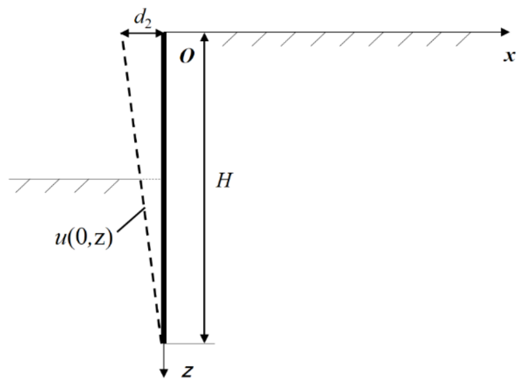

Fig. 6 R mode boundary condition

The normalized settlement induced by T mode can be expressed as:

$$\frac{w}{w_{\max}}=\frac{H^2\left(x_{ref}^{\ 2}+H^2\right)}{x_{ref}^{\ 2}}\left(\frac{1}{H^2}-\frac{1}{x_{ref}^{\ 2}+H^2}\right) \tag{29}$$

3.2 Rotation around the wall toe (R Mode)

The deformations at the top and the toe of the retaining wall are d2 and 0 respectively for R mode, as shown in Fig. 6.

Therefore,

$$u=\int_0^{+\infty}\frac{1}{\alpha}K_3\cos(\alpha\,z)\,\mathrm{d}\,\alpha=\frac{z}{H}d_2-d_2 \tag{30}$$

According to *Fourier* cosine integral transformation of $\frac{z}{H}d_2-d_2$, we get:

$$\frac{z}{H}d_2-d_2=\frac{2d_2}{\pi H}\int_0^{+\infty}\frac{\cos(H\alpha)-1}{\alpha^2}\cos(\alpha z)\,\mathrm{d}\,\alpha \tag{31}$$

Comparing Eq. (30) and Eq. (31), it is clear that

$$K_3=\frac{2d_2}{\pi H}\frac{\cos(H\alpha)-1}{\alpha} \tag{32}$$

Similar to the process from Eq. (20) and Eq. (23), the

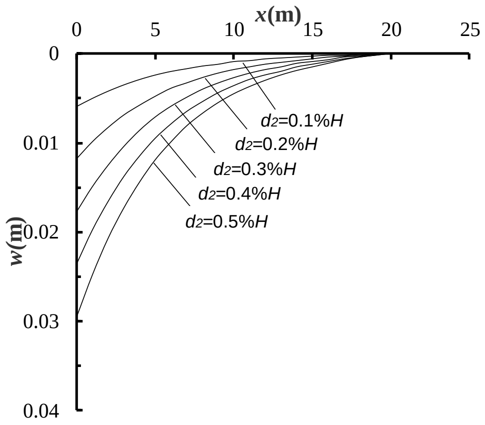

(a) Surface subsidence curves

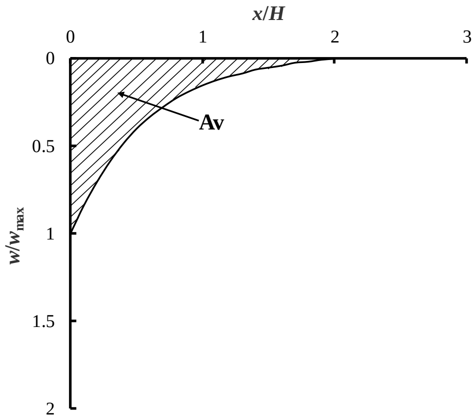

(b) Normalized curve of surface subsidence

Fig. 7 Distribution of surface subsidence caused by rotation around wall toe

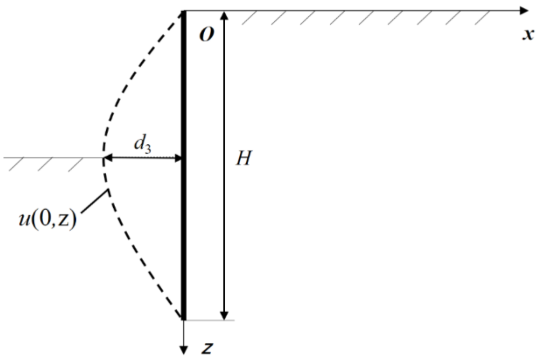

Fig. 8 Parabola boundaries of the retaining wall

normal stress at the surface can be expressed as following.

$$\sigma_{z|z=0} = -\frac{d_2 H}{\beta\pi}\frac{1}{x^2+H^2} - \frac{1}{4}\frac{d}{\pi H\beta}\ln\frac{x^4}{(x^2+H^2)^2} \tag{33}$$

Therefore, the positive vertical stress acting on the surface of the second part can be expressed in Eq. (34).

$$F(x) = \frac{d_2 H}{\beta\pi}\frac{1}{x^2+H^2} + \frac{1}{2}\frac{d_2}{\pi H\beta}\ln\frac{x^2}{x^2+H^2} \tag{34}$$

Substituting Eq. (34) into Eq. (25), the ground surface settlement induced by $F(x)$ is:

$$w(x) = -\frac{2d_2}{\pi^2}\int_{-\infty}^{+\infty}\left(\frac{H}{x_c^{\,2}+H^2} + \frac{1}{2H}\ln\frac{x_c^{\,2}}{x_c^{\,2}+H^2}\right)\ln\left|\frac{x_c - x}{x_c - x_{ref}}\right| \mathrm{d}\,x_c \tag{35}$$

Similar to the case mentioned in T mode section, the settlements and the normalized settlement calculated by Eq. (35) are shown in Fig.7. The distribution of the settlement induced by R mode is similar to that induced by T mode.

The normalized settlement induced by R mode can be expressed as following.

$$\frac{w(x)}{w_{\max}} = \frac{\left(x - x_{ref}\right)^2}{x_{ref}^2} \tag{36}$$

For undrained clay, assuming v=0.5. Thus, no ground loss occurs. The area covered by the surface settlement curve is equal to the area covered by the deflection curve of the retaining wall. As shown in Fig.6, the area covered by the deflection curve of the retaining wall, A_H, can be calculated by the following equation.

$$A_H = \frac{1}{2}Hd_2 \tag{37}$$

The area covered by the surface settlement curve, A_V, can be calculated:

$$A_V = \int_0^{x_{ref}} w(x)dx = \frac{1}{3}w_{\max}x_{ref} \tag{38}$$

As A_H=A_V, $w_{\max}$ can be obtained:

$$w_{\max} = \frac{3Hd_2}{2x_{ref}} \tag{39}$$

Obviously, the maximum settlement located at the location where x=0.

3.3 Parabola mode (P mode)

For parabola mode, the boundary condition at the retaining wall is $u(0,z) = \frac{4d_3}{H^2}z(z-H)$ when 0≤ z ≤H, as shown in Fig. 8.

Therefore,

$$u = \int_0^{+\infty}\frac{1}{\alpha}K_3\cos\alpha z d\alpha = \frac{4d_3}{H^2}z(z-H) \tag{40}$$

Through *Fourier* cosine integral transformation on $u(0,z)$, we get Eq. (37).

$$\frac{4d_3}{H^2}z(z-H) = \frac{1}{\pi}\int_0^{+\infty}\left(\frac{8d_3(1+\cos\alpha H)}{\alpha^2 H} - \frac{16d_3\sin\alpha H}{\alpha^3 H^2}\right)\cos\alpha z\mathrm{d}\alpha \tag{41}$$

By comparing Eq.(40) and Eq.(41), it can be found that:

$$K_3 = \frac{8d_3}{\pi H^2}\left[\frac{H(1+\cos\alpha H)}{\alpha} - \frac{2\sin\alpha H}{\alpha^2}\right] \tag{42}$$

Similar to the process from Eq.(20) and Eq.(23), the normal stress at the surface can be expressed as following.

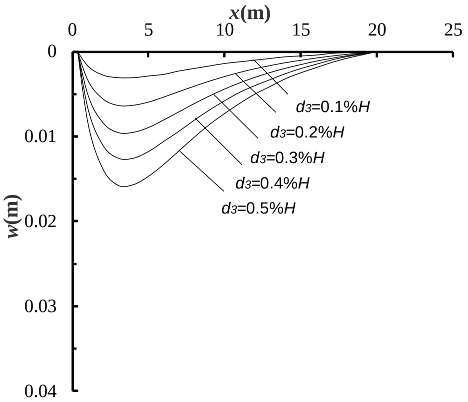

(a) Surface subsidence curves

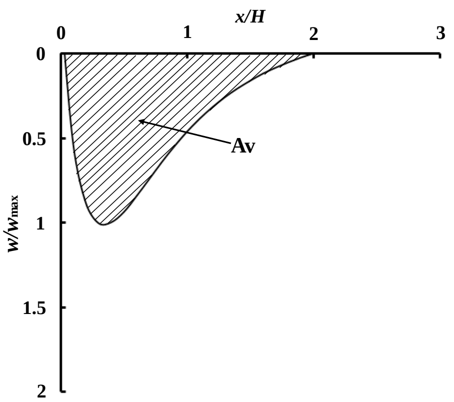

(b) Normalized curve of surface subsidence

Fig. 9 Surface subsidence distribution under parabola pattern

$$\sigma_{zd|z=0} = \frac{4d_3E}{(1-\upsilon^2)\pi H^2}(\frac{H}{2}\ln\frac{x^2}{x^2+H^2}+3H + \frac{Hx^2}{x^2+H^2} - 4x\arctan\frac{H}{x}) \tag{43}$$

The inversed surface pressure is:

$$F(x) = -\frac{4d_3E}{(1-\upsilon^2)\pi H^2}[\frac{H}{2}\ln\frac{x^2}{x^2+H^2}+3H + \frac{Hx^2}{x^2+H^2} - 4x\arctan\frac{H}{x}] \tag{44}$$

Substituting Eq. (44) into Eq. (25),

$$w(x) = -\frac{8d_3}{\pi^2H^2}\int_{-\infty}^{+\infty}(\frac{H}{2}\ln\frac{x_c{}^2}{x_c{}^2+H^2}+3H+\frac{Hx_c{}^2}{x_c{}^2+H^2} - 4x_c\arctan\frac{H}{x_c})\ln\left|\frac{x_c-x}{x_c-x_{ref}}\right|dx_c \tag{45}$$

Calculating the case mentioned in T mode section, the surface settlements and the normalized settlement calculated by Eq. (45) are shown in Fig. 9.

According to Fig. 8, the area covered by the deflection curve of the retaining wall, A_H, can be calculated as:

$$A_H = \int_0^{d_3} u(0,z)dz = -\int_0^{d_3}\frac{4d_3}{H^2}z(z-H)dz = \frac{2d_3^3(3H-2d_3)}{3H^2} \tag{46}$$

According to Fig. 9 and Eq. (45), the area covered by the surface settlement curve, A_V, can be calculated as:

$$A_V = \int_0^{x_{ref}} w(x)dx = \int_0^{4i} w(x)dx \approx \int_{-\infty}^{+\infty} w(x)dx \tag{47}$$

As A_H=A_V, $w_{\max}$ can be obtained:

$$w_{\max} = \frac{3.2d_3^3(3H-2d_3)}{3H^2x_{ref}} \tag{48}$$

Let the first derivative of $w(x)$ equals 0, the location where the maximum settlement occurs can be obtained by numerical method, x=x_{ref}/4=H/2.

In summary, the combination of T mode, R mode and P mode could form a common deformation mode of retaining wall in practice. Then the ground settlement induced by the excavation can be obtained in practice.

4. Verification

To verify the rationality of the proposed analytical solution, four excavation cases reported by Hsieh and Ou (1998) were analyzed by the proposed method in this paper.

Case 1 is located near the center of the Taipei basin. The soil conditions consist mainly of silty clay, the profile of the soil is shown in Fig. 10(a). The average undrained shear strength of soft clay is 80 kPa. The diaphragm wall depth is 35m. The excavation depth is 19.7m. The excavation width is 41m. The excavation is excavated in 7 steps using top-down method. The observed maximum horizontal deformation of the retaining wall is 0.54%H.

Case 2 is also located in the Taipei basin. The ground condition is mainly composed of silty clay overlying clayey silt. The average undrained strength of soft clay is 55 kPa. The diaphragm wall length is 31m. The excavation depth is 18.45m. The excavation width is 35m. The excavation is excavated in 7 steps using bottom-up method. The observed maximum horizontal deformation of the retaining wall is 0.34%H.

Case 3 is the New Palace Yard Park project in London. The foundation soil is stiff London clay. The average undrained strength of the soft clay is 170 kPa. The diaphragm wall length is 30 m. The excavation depth is 18.5m. The excavation width is 50 m. The excavation is excavated in 6 steps using bottom-up method. The observed maximum horizontal deformation of the retaining wall is 0.13%H.

Case 4 is the Bell Common Tunnel in England. The subsurface soil is mainly London clay. The average undrained strength of the soft clay is 150 kPa. The Secant pile wall length is 21 m. The excavation depth is 9 m. The excavation width is 40 m. The excavation is excavated in 2 steps using bottom-up method. The observed maximum horizontal deformation of the retaining wall is 0.29%H.

As shown in Fig.10, the calculated results fit the measured data very well. Both the maximum settlement and the location where the maximum settlement occurs are predicted reasonably. The larger prediction in Fig. 10(d)

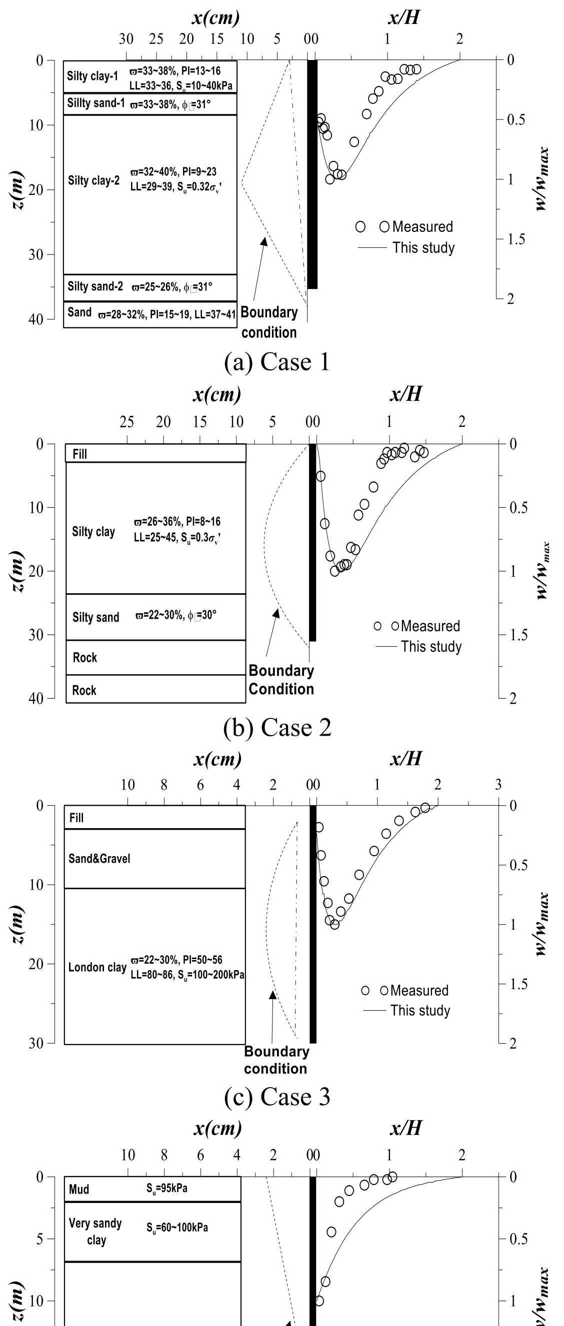

(a) Case 1

(b) Case 2

(c) Case 3

(d) Case 4

Fig. 10 Deformation of foundation pits and normalized curves of surface subsidence

may due to the assumption that the influence area is equal to $2H$. While, it seem the influence area in this case is H based on the measured data.

5. Discussion

According to the equations, it is clear that the settlements are independent on elastic modulus of soils. We think the soil modulus would not influence the distribution of the soil deformations for a displacement-controlled boundary problem. Several cases are analyzed by FEM to verify the assumption. For those cases, excavation depth is set as 5 m, retaining wall length is set as 10 m. Elastic

Table 1 Information of the cases with different modulus

Deformation mode	H	ν=0.5		
		E_1	E_2	E_3
T mode	10m	10MPa	20MPa	30MPa
R mode	10m	10MPa	20MPa	30MPa
P mode	10m	10MPa	20MPa	30MPa

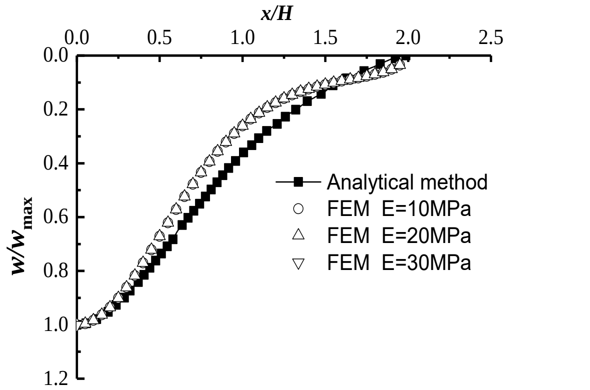

Fig. 11 Normalized curve calculated by analytical method and FEM under T mode

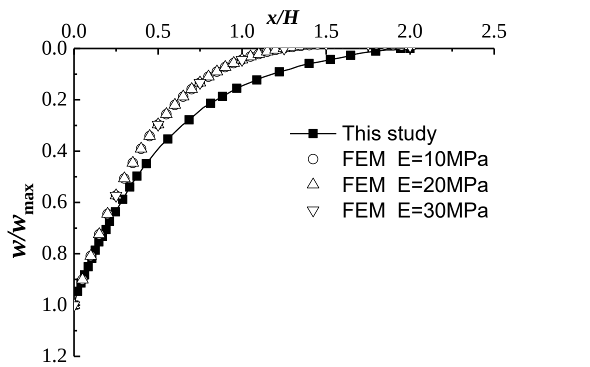

Fig. 12 Normalized curve calculated by analytical method and FEM under R mode

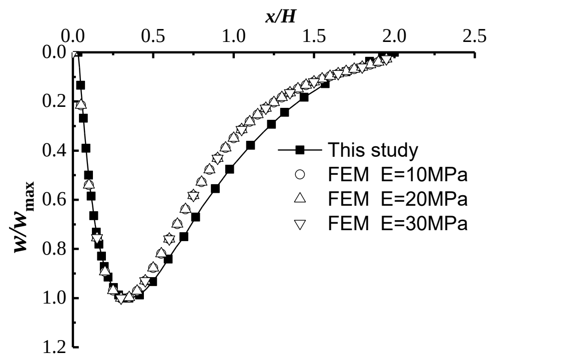

Fig. 13 Normalized curve calculated by analytical method and FEM under P mode

model is used for the soil. The Poisson's Ratio of the soil is 0.499. The other information of the cases are shown in Table 1. The settlements calculated by the analytical method and FEM can be seen in Fig. 11, Fig. 12 and Fig. 13. It is clear that the soil movement is only relative to the boundary condition while using displacement-controlled method. The elastic modulus of the soil will not influence the soil movement induced by the excavation in a displacement-controlled analysis. However, the maximum deformation of the wall, which we assumed as the boundary condition, would be decided by the soil parameters. The conclusion is consistent with the formula proposed for calculating the ground settlement induced by tunneling by Loganathan and Poulos (1998).

6. Conclusions

Three basic solutions for ground settlement induced by excavations are obtained according to T mode, R mode and P mode respectively through elastic theory coupled with mirror symmetry principle. T mode and R mode would result in spandrel type settlement, while P model would result in concave type settlement. The ground deformation induced by the excavation in practice can be obtained by combining those three ingredients. The validation shows the analytical method can calculate the ground settlement induced by the excavation reasonably based on the known wall deflection.

Acknowledgments

The authors gratefully acknowledge financial support by the National Natural Science Foundation of China (Grand No. 51738010), the National Key R&D Program (Grant No. 2016YFC0800200), Shanghai Science and Technology Committee Rising-Star Program(19QC1400500) and the Fundamental Research Funds for the Central Universities(22120190220).

References

Arai, Y., Kusakabe, O., Murata, O. and Konishi, S. (2008), "A numerical study on ground displacement and stress during and after the installation of deep circular diaphragm walls and soil excavation", *Comput. Geotech.*, **35**(5), 791-807. https://doi.org/10.1016/j.compgeo.2007.11.001.

Chen, Y., Zhao, W., Jia, P. and Han, J. (2018), "Proportion analysis of ground settlement caused by excavation and dewatering of a deep excavation in sand area", *Indian Geotech. J.*, **48**(1), 103-113. https://doi.org/10.1007/s40098-017-0249-3.

Cheng, C.Y., Dasari, G.R., Chow, Y.K. and Leung, C.F. (2007), "Finite element analysis of tunnel–soil–pile interaction using displacement controlled model", *Tunn. Undergr. Sp. Technol.*, **22**(4), 450-466. https://doi.org/10.1016/j.tust.2006.08.002.

Clough, G.W. and O'Rourke, T.D. (1990), "Construction induced movements of in-situ walls", *Geotech. Special Publ.*, **25**, 439-470.

DG/TJ08-61-2010 (2010), *Technical Code for Excavations Engineering*, Shanghai Engineering Construction Code, Shanghai, China.

Finno, R.J. and Bryson, L.S. (2002), "Response of a building adjacent to stiff excavation support system in soft clay", *J. Perform. Construct. Facilit.*, **16**(1), 10-20. https://doi.org/10.1061/(ASCE)0887-3828(2002)16:1(10).

Finno, R.J. and Harahap, I.S. (1991), "Finite element analyses of HDR-4 excavation", *J. Geotech. Eng.*, **117**(10), 1590-1609. https://doi.org/10.1061/(ASCE)0733-9410(1991)117:10(1590).

Golpasand, M.R.B., Nikudel, M.R. and Uromeihy, A. (2016), "Specifying the real value of volume loss (VL) and its effect on ground settlement due to excavation of Abuzar tunnel, Tehran", *Bull. Eng. Geol. Environ.*, **75**(2), 1-17. https://doi.org/10.1007/s10064-015-0788-8.

Hashash, Y.M. and Whittle, A.J. (1996), "Ground movement prediction for deep excavations in soft clay", *J. Geotech. Eng.*, **122**(6), 474-486. https://doi.org/10.1061/(ASCE)0733-9410(1996)122:6(474).

He, P., Xu, Z., Wang, W. and Li, Z. (2018), "Observed performance of an ultra large deep excavation in shanghai soft clay", *Proceeding of the GeoShanghai International Conference*, Shanghai, China, May.

Hong, Y., Ng, C.W.W., Liu, G.B. and Liu, T. (2015), "Three-dimensional deformation behaviour of a multi-propped excavation at a "greenfield" site at Shanghai soft clay", *Tunn. Undergr. Sp. Technol.*, **45**, 249-259. https://doi.org/10.1016/j.tust.2014.09.012.

Hsieh, P.G. and Ou, C.Y. (1998), "Shape of ground surface settlement profiles caused by excavation", *Can. Geotech. J.*, **35**(6), 1004-1017. https://doi.org/10.1139/cgj-35-6-1004.

Kang, I., Lee, H. and Kim, T. (2017), "Accurate estimation of ground settlement behind excavation support wall using conditional merging", *Proceedings of the 2017 Spring Geosynthetics Conference*, Santiago, Chile, July.

Kim, T. and Jung, Y. (2016), "Accurate estimation of settlement profile behind excavation using conditional merging technique", *J. Kor. Geoenviron. Soc.*, **17**(8), 39-44. https://doi.org/10.14481/jkges.2016.17.8.39.

Kung, G.T., Juang, C.H., Hsiao, E.C. and Hashash, Y.M. (2007), "Simplified model for wall deflection and ground-surface settlement caused by braced excavation in clays", *J. Geotech. Geoenviron. Eng.*, **133**(6), 731-747. https://doi.org/10.1061/(ASCE)1090-0241(2007)133:6(731).

Kyrou, K. (1980), "The effect of trench excavation induced ground movements on adjacent buried pipelines", Ph.D. Dissertation, University of Surrey, Guildford, U.K.

Lam, S.Y. (2010), "Ground movements due to excavation in clay: physical and analytical models", Ph.D. Dissertation, University of Cambridge, Cambridge, U.K.

Liu, J., Zhou, D. and Liu, K. (2015), "A mathematical model to recover missing monitoring data of foundation pit", *Geomech. Eng.*, **9**(3), 275-286. https://doi.org/10.12989/gae.2015.9.3.275.

Loganathan, N. and Poulos, H.G. (1998), "Analytical prediction for tunnelling-induced ground movement in clays", *J. Geotech. Geoenviron. Eng.*, **124**(9), 846-856. https://doi.org/10.1061/(ASCE)1090-0241(1998)124:9(846).

Mu, L., Finno, R.J., Huang, M., Kim, T. and Kern, K. (2015), "Defining the soil parameters for computing deformations caused by braced excavation", *Maejo Int. J. Sci. Technol.*, **9**(02), 165-180. https://doi.org/10.14456/mijst.2015.14.

Mu, L. and Huang, M. (2016), "Small strain based method for predicting three-dimensional soil displacements induced by braced excavation", *Tunn. Undergr. Sp. Technol.*, **52**, 12-22. https://doi.org/10.1016/j.tust.2015.11.001.

Mu, L., Huang, M. and Finno, R.J. (2012), "Tunnelling effects on lateral behavior of pile rafts in layered soil", *Tunn. Undergr. Sp.*

Technol., **28**, 192-201. https://doi.org/10.1016/j.tust.2011.10.010.
Ou, C.Y. and Hsieh, P.G. (2011), "A simplified method for predicting ground settlement profiles induced by excavation in soft clay", *Comput*. *Geotech*., **38**(8), 987-997. https://doi.org/10.1016/j.compgeo.2011.06.008.
Ou, C.Y., Hsieh, P.G. and Chiou, D.C. (1993), "Characteristics of ground surface settlement during excavation", *Can*. *Geotech*. *J*., **30**(5), 758-767. https://doi.org/10.1139/t93-068.
Pasternak, E., Mühlhaus, H.B. and Dyskin, A.V. (2004), "On the possibility of elastic strain localisation in a fault", *Pure Appl*. *Geophys*., **161**(11-12), 2309-2326. https://doi.org/10.1007/s00024-004-2565-7.
Poulos, H.G. (1997), "Failure of a building supported on piles", *Proceedings of the International Conference on Foundation Failures*, Singapore, May.
Poulos, H.G. and Davis, E.H. (1974), *Elastic Solutions for Soil and Rock Mechanics*, John Wiley & Sons, Inc., New York, U.S.A.
Roboski, J. and Finno, R.J. (2006), "Distributions of ground movements parallel to deep excavations in clay", *Can*. *Geotech*. *J*., **43**(1), 43-58. https://doi.org/10.1139/T05-091.
Seok, J.W., Kim, O.Y., Chung, C.K. and Kim, M.M. (2001), "Evaluation of ground and building settlement near braced excavation sites by model testing", *Can*. *Geotech*. *J*., **38**(5), 1127-1133. https://doi.org/10.1139/cgj-38-5-1127.
Sheehan, A.J., Olson, R.E., Park, K. and Stokoe, II, K.H. (2010), "Estimation of settlement of footings under working loads using equivalent-linear elasticity", *Proceedings of the GeoFlorida 2010: Advances in Analysis, Modeling & Design*, Orlando, Florida, U.S.A., February.
Tan, Y., Zhu, H., Peng, F., Karlsrud, K. and Wei, B. (2012), "Characterization of semi-top-down excavation for subway station in Shanghai soft ground", *Tunn*. *Undergr*. *Sp*. *Technol*., **68**, 244-261. https://doi.org/10.1016/j.tust.2017.05.028.
Wang, L., Ravichandran, N. and Juang, C.H. (2012a), "Bayesian updating of KJHH model for prediction of maximum ground settlement in braced excavations using centrifuge data", *Comput*. *Geotech*., **44**, 1-8. https://doi.org/10.1016/j.compgeo.2012.03.003.
Wang, W.D., Wang, H.R. and Xu, Z.H. (2012b), "Simplified method of deformation prediction for excavations retained by embedded walls in Shanghai soft soil", *Chin*. *J*. *Geotech*. *Eng*., **34**(10), 1792-1800.
Wang, J.H., Xu, Z.H. and Wang, W.D. (2009), "Wall and ground movements due to deep excavations in Shanghai soft soils", *J*. *Geotech*. *Geoenviron*. *Eng*., **136**(7), 985-994. https://doi.org/10.1061/(ASCE)GT.1943-5606.0000299.
Zahmatkesh, A. and Choobbasti, A.J. (2015), "Evaluation of wall deflections and ground surface settlements in deep excavations", *Arab*. *J*. *Geosci*., **8**(5), 3055-3063. https://doi.org/10.1007/s12517-014-1419-6.
Zapata, M.D. (2007), "Semi-empirical method for designing excavation support systems based on deformation control", Master Dissertation, University of Kentucky, Lexington, Kentucky, U.S.A.
Zheng, G. and Li, Z.W. (2012), "Comparative analysis of responses of buildings adjacent to excavations with different deformation modes of retaining walls", *Chin*. *J*. *Geotech*. *Eng*., **34**(6), 969-977.

CC

Notations

H	wall length
$u(0,z)$	horizontal deformation of the retaining wall
d_1	maximum horizontal deformation of the retaining wall under translation
d_2	maximum horizontal deformation of the retaining wall under rotation
d_3	maximum horizontal deformation of the retaining wall under parabola deformation
σ_{xz}	normal stress
λ	first Lame's elastic coefficients
G	second Lame's elastic coefficients
E	elastic modulus of soil
υ	Poisson's ratio of soil
u	horizontal displacement
w	vertical displacement
θ	volumetric strain
ω	rigid body rotation angle
K_1	coefficients depend on the boundary conditions
A	coefficients depend on the boundary conditions
K_3	coefficients depend on the boundary conditions
$w_1(x,0)$	vertical displacement at the surface of part 1
$w_2(x,0)$	vertical displacement at the surface of part 2
$F(x)$	inverse stress acting on the surface in part 2
x_{ref}	x coordinate of the reference point where ground settlement induced by the excavation usually occurs in a zone
P	concentrated load on the surface
s	distance from the concentrated load to the reference point
ρ	distance from the concentrated load to the calculation point
x_c	x coordinate of the point where the concentrated load is applied
x	x coordinate of the calculation point

w_{max}	maximum settlement
A_H	area covered by the deflection curve of the retaining wall
A_V	area covered by the surface settlement curve
ϖ	water content
PI	plasticity index
LL	liquid limit
ϕ'	drained friction angle
σ_v'	effective overburden pressure
S_u	undrained shear strength